




Curvaton-assisted hilltop inflation

Wen-Yuan Ai ^{1,2,*} Stephen F. King ^{3,†} Xin Wang ^{3,4,5,‡} and Ye-Ling Zhou ^{6,§}

¹*State Key Laboratory of Dark Matter Physics,
Tsung-Dao Lee Institute and School of Physics and Astronomy,
Shanghai Jiao Tong University, Shanghai 201210, China*

²*Key Laboratory for Particle Astrophysics and Cosmology (MOE),
and Shanghai Key Laboratory for Particle Physics and Cosmology,
Shanghai Jiao Tong University, Shanghai 201210, China*

³*School of Physics and Astronomy, University of Southampton, Southampton SO17 1BJ, United Kingdom*

⁴*Dipartimento di Fisica e Astronomia “Galileo Galilei”,
Università degli Studi di Padova, Via Francesco Marzolo 8, 35131 Padova, Italy*

⁵*INFN, Sezione di Padova, Via Francesco Marzolo 8, 35131 Padova, Italy*

⁶*School of Fundamental Physics and Mathematical Sciences,
Hangzhou Institute for Advanced Study, UCAS, Hangzhou 310024, China*

(Dated: May 12, 2026)

Following the recent Atacama Cosmology Telescope (ACT) results, we consider hilltop inflation where the inflaton is coupled to a curvaton, simultaneously addressing two main challenges faced by conventional hilltop inflation models: the initial-value problem; and their viability for sub-Planckian field values. In standard single-field hilltop inflation, the inflaton must start extremely close to the maximum of the potential, raising concerns about the naturalness of the initial conditions. We demonstrate that the curvaton field not only significantly relaxes the initial-value tuning required for hilltop inflation, but also opens up parameter space through modifying the curvature perturbation power spectrum, reviving the *quartic* hilltop inflation model in the sub-Planckian regime. We find viable parameter space consistent with the recent cosmological observations.

I. INTRODUCTION

Precision measurements of primordial curvature perturbations have established a spectrum that is almost scale-invariant, predominantly adiabatic and close to Gaussian, with a small red tilt [1–3]. This strongly favors the inflationary paradigm, in which a scalar field (the inflaton) slowly rolls along a very flat region of its potential [4–7].

Recently, the most up-to-date Atacama Cosmology Telescope (ACT) DR6 analysis has reported a spectral index of $n_s = 0.9743 \pm 0.0034$ based on a joint fit with Planck and the Dark Energy Spectroscopic Instrument (DESI) DR1 data [8]. This value differs from the original Planck18 (TT,TE,EE+lowE) result $n_s = 0.9649 \pm 0.0044$ [2] by about 2σ and has triggered a lot of discussions on inflationary models, see, e.g., Refs. [9–30].

In the context of inflationary model building, hilltop inflation [6, 7, 31–33] constitutes an attractive class of models, in which inflation is driven by a scalar field ϕ rolling down from the vicinity of an unstable local maximum of the potential, which can be parametrized near the hilltop as

$$V(\phi) = \Lambda^4(1 - \phi^p/\mu^p + \dots), \quad (1)$$

where Λ and μ are characteristic energy scales, and $p \geq 2$ denotes an integer. Recently, it has been shown that hilltop inflation can be realized in a modular-invariant framework if the inflaton is identified with a modulus field [34, 35]. The *quadratic* case ($p = 2$) is viable only as a large-field inflation model with $\mu \gtrsim M_{\text{Pl}}$. By contrast, for the *cubic* ($p = 3$) and *quartic* ($p = 4$) hilltop potentials, the entire sub-Planckian regime ($\mu \lesssim M_{\text{Pl}}$) already lies outside the 95% confidence level (C.L.) region of the Planck constraints [2].

On the other hand, since the inflation is required to start extremely close to the hilltop of the potential, hilltop inflation clearly faces an initial condition problem. In Ref. [36], this problem was addressed by introducing a pre-inflationary stage during which a matter field undergoes classical slow-roll evolution and dynamically drags the inflaton toward the suitable initial position for the subsequent hilltop inflationary phase.

In this work, motivated by these problems, we consider a curvaton-assisted hilltop scenario in which the inflaton is coupled to a light scalar field σ , whose dynamics in the pre-inflationary era is dominated by quantum diffusion. We track the evolution of σ and ϕ during the pre-inflationary stage by solving the Langevin equations in the quantum-diffusion region, and derive analytically a characteristic onset window for hilltop inflation that is only weakly sensitive to the initial value of σ . Once hilltop inflation starts, σ becomes effectively frozen and plays the role of a curvaton [37–41], modifying curvature perturbations upon the curvaton decay at later times after inflation and alleviating the tension of conventional hilltop models with current Cosmic Microwave

* wenyuanai@sjtu.edu.cn

† king@soton.ac.uk

‡ xin.wang@unipd.it

§ zhouyeling@ucas.ac.cn

Background (CMB) observations. We perform an illustrative Bayesian analysis based on a simplified likelihood constructed from the Planck and ACT results, assessing and comparing how well our model is supported by each of them. From the resulting posterior distributions, we further present the model predictions for the tensor-to-scalar ratio and primordial non-Gaussianity. We demonstrate that the curvaton field not only significantly relaxes the initial-value tuning of hilltop inflation, but also opens up parameter space through modifying the curvature perturbation power spectrum, reviving the *quartic* hilltop inflation models in the sub-Planckian regime.

The layout of the remainder of this paper is as follows. We construct our model in Sec. II. In Sec. III, we derive the initial conditions for hilltop inflation. In Sec. IV, we discuss how the curvaton mechanism modifies the primordial observables in hilltop inflation. In Sec. V, we show the results of our Bayesian analysis and discuss their implications. We summarize our main conclusions in Sec. VI. In appendices A and B, we provide additional technical details of Langevin equations and the δN formalism. In appendix C, we discuss the viability of the *cubic* hilltop case.

II. HILLTOP INFLATION WITH A CURVATON

We consider a two-field scalar potential involving an inflaton ϕ and a curvaton σ . ϕ drives hilltop inflation during the slow-roll phase, whereas σ modifies the power spectrum of primordial perturbations after inflation. The scalar potential can be expressed in a general form as

$$V = V_{\text{HT}} + V_{\text{S}} + V_{\text{C}} , \quad (2)$$

where V_{HT} denotes the primary hilltop potential [6, 7]

$$V_{\text{HT}} = \Lambda^4 \left(1 - \frac{\phi^p}{2\mu^p} \right)^2 , \quad (3)$$

where a factor of two is added in the denominator to be consistent with eq. (1). In this paper, we focus on two specific examples: $p = 3$ (*cubic* hilltop inflation) and $p = 4$ (*quartic* hilltop inflation).

The soft term in eq. (2) is given by

$$V_{\text{S}} = -\frac{1}{2}m_\phi^2\phi^2 + \frac{1}{2}m_\sigma^2\sigma^2 , \quad (4)$$

with m_ϕ and m_σ being the bare masses of ϕ and σ , respectively. Note that m_σ^2 should be much smaller than the Hubble parameter $H^2 \approx V/(3M_{\text{Pl}}^2)$ during inflation to ensure that the curvaton σ is effectively frozen.

Finally, we use V_{C} to represent the cross term between ϕ and σ , which is chosen to be

$$V_{\text{C}} = \frac{\lambda^2}{2M_{\text{Pl}}^2}\phi^2\sigma^4 , \quad (5)$$

where λ is a dimensionless coupling constant and $M_{\text{Pl}} \equiv 2.435 \times 10^{18}$ GeV is the reduced Planck mass. V_{C} contributes to the effective mass of ϕ and modulates the shape of the potential along the ϕ -direction. To be more specific, we assume that σ starts from a sufficiently large value, so that the effective mass $m_{\phi,\text{eff}}^2 = \lambda^2\sigma^4/M_{\text{Pl}}^2 - m_\phi^2 > 0$ and $\phi = 0$ is a minimum in the ϕ -direction. As σ moves close to the critical value $\sigma_c = (m_\phi M_{\text{Pl}}/\lambda)^{1/2}$, $\phi = 0$ transitions from a local minimum to a saddle point, which naturally sets the stage for the subsequent hilltop inflation.

Before going to the next section, we shall mention that the scalar potential discussed above could originate from supersymmetry. To be more specific, V_{HT} and V_{C} can be derived from the following superpotential

$$W = \widehat{S}_1 \left(\frac{\widehat{\Phi}^p}{M^{p-2}} - \Lambda^2 \right) + \frac{2\lambda}{M_{\text{Pl}}} \widehat{S}_2 \widehat{\Phi} \widehat{X}^2 , \quad (6)$$

where \widehat{S}_1 , \widehat{S}_2 , $\widehat{\Phi}$ and \widehat{X} are the superfields, and M is a mass parameter. These superpotential terms are enforced by arranging S_1 and S_2 to have R -charge 2 and imposing an additional Z_p symmetry with suitable charges for \widehat{S}_2 , $\widehat{\Phi}$ and \widehat{X} . It is straightforward to identify that $V_{\text{HT}} = |\partial W/\partial \widehat{S}_1|^2$ and $V_{\text{C}} = |\partial W/\partial \widehat{S}_2|^2$ given the relations $\phi = \sqrt{2}\text{Re } \Phi$, $\sigma = \sqrt{2}|X|$ (with Φ and X being the scalar components of $\widehat{\Phi}$ and \widehat{X} , respectively) and $\mu^p = 2^{p/2-1}M^{p-2}\Lambda^2$, whereas V_{S} is attributed to soft supersymmetry breaking corrections.

III. INITIAL CONDITIONS FOR HILLTOP INFLATION

In the vicinity of $\phi = 0$, the evolution of ϕ is dominated by the quantum fluctuations, giving rise to a quantum diffusion region whose width depends on the value of σ . Within one Hubble time, the typical displacement of ϕ induced by quantum diffusion is given by $\delta\phi_{\text{q}} \simeq H/(2\pi)$, while the displacement due to the classical drift can be estimated as $\delta\phi_{\text{cl}} \simeq |V_\phi|/(3H^2)$ with $V_\phi \equiv \partial V/\partial\phi$. The boundary ϕ_{b} of the diffusion region can be roughly determined by equating $\delta\phi_{\text{q}}$ and $\delta\phi_{\text{cl}}$, namely,

$$\frac{H}{2\pi} = M_{\text{Pl}}^2 \left| \frac{V_\phi}{V} \right|_{\phi_{\text{b}}} , \quad (7)$$

where

$$V_\phi = m_\phi^2 \left(\frac{\sigma^4}{\sigma_c^4} - 1 \right) \phi - p\Lambda^4 \frac{\phi^{p-1}}{\mu^p} + \dots , \quad (8)$$

and “ \dots ” denotes higher-order corrections. We identify the onset of hilltop inflation with the exit of ϕ from the diffusion region. The first step is therefore to determine the value of σ at which ϕ leaves the diffusion region and its dynamics becomes classical.

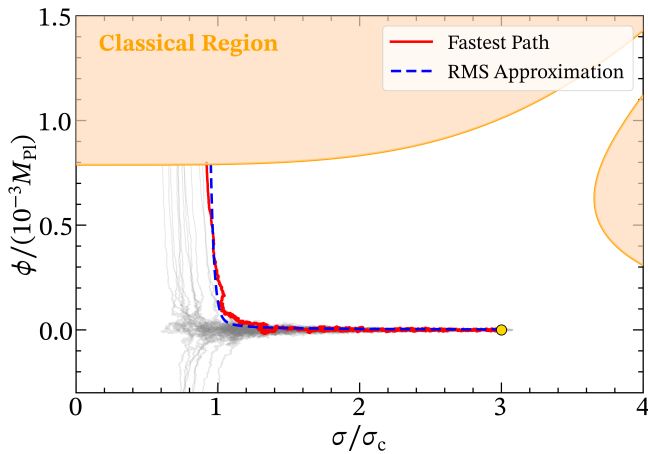


FIG. 1: Comparison between the stochastic paths of fields using the Markov-chain Monte Carlo (MCMC) simulation and the root-mean-square (RMS) approximation in the *quartic* hilltop model, where we set $\Lambda = 3 \times 10^{-4} M_{\text{Pl}}$, $\mu = 0.7 M_{\text{Pl}}$, $\lambda = 2 \times 10^{-4}$, $m_\phi = 3 \times 10^{-11} M_{\text{Pl}}$ and $m_\sigma = 5 \times 10^{-12} M_{\text{Pl}}$. The gray lines depict the field trajectories initialized at the yellow point ($\phi_0 = 0, \sigma_0 = 3\sigma_c$), and terminated once they cross into the classical region [$M_{\text{Pl}}^2 |V_\phi/V| > H/(2\pi)$], indicated by the orange shading. The solid red line denotes the fastest escaped trajectory. The dashed blue curve represents the RMS-approximated path, obtained by solving the Langevin equations in terms of mean-square values of the fields.

The evolution of ϕ and σ inside the diffusion region is described by the following Langevin equations [42–44]

$$\frac{d\phi}{dN} = -\frac{V_\phi}{3H^2} + \frac{H}{2\pi} \xi_\phi(N), \quad (9)$$

$$\frac{d\sigma}{dN} = -\frac{V_\sigma}{3H^2} + \frac{H}{2\pi} \xi_\sigma(N), \quad (10)$$

where $V_\sigma \equiv \partial V/\partial\sigma$, and we use the number of e-folds N as the time variable. The first terms on the right-hand sides represent classical drift, and the second terms are the stochastic “kicks” from quantum diffusion with $\xi_\phi(N)$ and $\xi_\sigma(N)$ being independent Gaussian white noise terms with zero mean and unit variance, i.e., $\langle \xi_i(N)\xi_j(N') \rangle = \delta_{ij}\delta(N-N')$. It should be mentioned that, unlike Ref. [36] where the pre-inflationary direction is taken as a slow-roll direction dominated by classical drift, the curvaton direction of interest can be dominated by quantum diffusion since we require $m_\sigma \ll H$. In this case, quantum fluctuations may occasionally kick σ back to larger field values, so that in certain Hubble patches inflation could keep taking place, leading to the paradigm of eternal inflation [45]. In the present work, we treat eternal inflation as an open question, noting that such behavior is in fact already a generic feature of single-field hilltop inflation models [46].

The Langevin equations given in eqs. (9) and (10) can be numerically solved using a Markov-chain Monte Carlo

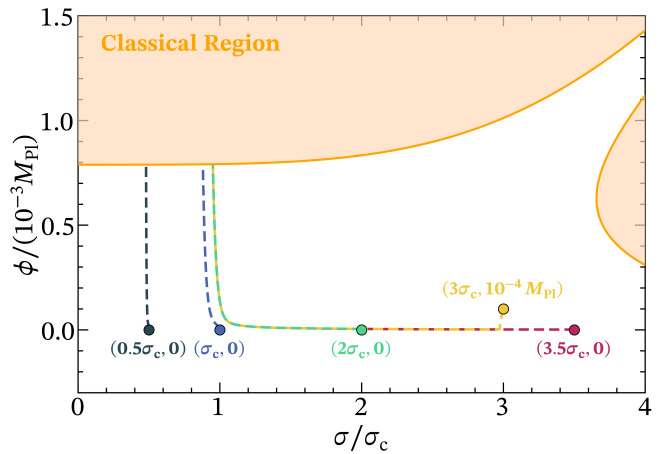


FIG. 2: The RMS-approximated paths for different starting points in the *quartic* hilltop model. Model parameters in the scalar potential take the same values as those in Fig. 1.

(MCMC) approach. To be specific, we start a large ensemble of trajectories from an initial point with $\phi_0 = 0$ and $\sigma_0 \gtrsim \sigma_c$. We track these trajectories until the first time they cross the diffusion boundary defined by eq. (7), with the additional constraint that $V_\phi < 0$ to ensure the onset of hilltop inflation. Taking the *quartic* hilltop model for instance, we show the simulation results in Fig. 1. All the gray trajectories presented in Fig. 1 start from the same point ($\phi_0 = 0, \sigma_0 = 3\sigma_c$), and terminate once they first reach the diffusion boundary satisfying eq. (7). Since we are particularly interested in the paths that cross into the classical region at earlier times, we highlight the fastest escaped trajectory in red.

By averaging Langevin equations over many realizations of the stochastic process, one can obtain equations for the mean-square values of the fields $\langle \phi^2 \rangle$ and $\langle \sigma^2 \rangle$ as

$$\frac{d\langle \phi^2 \rangle}{dN} = -\frac{2}{3H^2} \langle V_\phi \cdot \phi \rangle + \left(\frac{H}{2\pi} \right)^2, \quad (11a)$$

$$\frac{d\langle \sigma^2 \rangle}{dN} = -\frac{2}{3H^2} \langle V_\sigma \cdot \sigma \rangle + \left(\frac{H}{2\pi} \right)^2. \quad (11b)$$

For the parameter region of interest, the covariance between ϕ and σ can be safely neglected. Furthermore, given that the fields start with $\phi_0 \approx 0$ and $\sigma_0 \gtrsim \sigma_c$, the above equations can be approximated by

$$\frac{d\langle \phi^2 \rangle}{dN} \approx -\frac{2}{3H^2} (C_1 \langle \phi^2 \rangle + C_2 \langle \phi^2 \rangle^2) + \left(\frac{H}{2\pi} \right)^2, \quad (12a)$$

$$\frac{d\langle \sigma^2 \rangle}{dN} \approx -\frac{2m_\sigma^2}{3H^2} \langle \sigma^2 \rangle - \frac{4\lambda^2 \langle \phi^2 \rangle \langle \sigma^4 \rangle}{3H^2 M_{\text{Pl}}^2} + \left(\frac{H}{2\pi} \right)^2, \quad (12b)$$

where

$$C_1 = m_\phi^2 \left(\frac{\langle \sigma^4 \rangle}{\sigma_c^4} - 1 \right), \quad C_2 = -\frac{27\Lambda^8}{m_\phi^2 \mu^6} \left(\frac{\langle \sigma^4 \rangle}{\sigma_c^4} - 1 \right)^{-1}, \quad (13)$$

for $p = 3$, and

$$C_1 = m_\phi^2 \left(\frac{\langle \sigma^4 \rangle}{\sigma_c^4} - 1 \right), \quad C_2 = -\frac{12\Lambda^4}{\mu^4}. \quad (14)$$

for $p = 4$. A detailed derivation of eqs. (11a)–(14) can be found in appendix A. Note that here we take $\langle \sigma^4 \rangle \simeq \langle \sigma^2 \rangle^2$, provided that σ starts from a large value and follows an approximate Gaussian distribution.

In this formalism, the explicit noise dependence can be removed, and the competition between the diffusive source term and the classical drift term becomes manifest. We can approximately regard the positions of ϕ and σ at a given time as their respective root-mean-square (RMS) values, namely, $\phi \simeq \phi_{\text{rms}} = \sqrt{\langle \phi^2 \rangle}$ and $\sigma \simeq \sigma_{\text{rms}} = \sqrt{\langle \sigma^2 \rangle}$. Taking the *quartic* hilltop model as an example, we numerically solve eqs. (12a) and (12b), and obtain an RMS-approximated path, which is denoted by the blue dashed curve in Fig. 1. The RMS-approximated path agrees well with the successfully escaped paths obtained from MCMC, in particular the fastest one, indicating that it can be used to represent the stochastic behavior of the fields in the diffusion region.

We further present the RMS-approximated paths starting from different points in Fig. 2. It is easy to see that for starting points with $\sigma_0 \lesssim 1.1\sigma_c$, ϕ rapidly diffuses to the boundary, while σ diffuses slowly. Nevertheless, if we start at some points where $\sigma_0 \gtrsim 1.1\sigma_c$, we can clearly observe an “L-shaped” path: when σ is large, ϕ is trapped near $\phi = 0$ by its large positive effective mass, and its evolution is strongly suppressed; once σ approaches $1.1\sigma_c$, ϕ starts to diffuse rapidly. It is interesting that such transitions occur before σ reaches σ_c , because the second term on the right-hand side of eq. (8) can provide a sizable negative contribution for large ϕ , given the large value of Λ in our model. In this case, even if the effective mass of ϕ at $\phi = 0$ remains positive, large quantum fluctuations can push the field over the barrier into the hilltop inflationary region, known as stochastic tunneling [47–51].

In fact, the “L-shaped” transition can be understood from the properties of Langevin equations for the field mean-square values. Before the turning point of the “L-shaped” trajectory, $\phi \simeq 0$. Then for the evolution of σ , the first term on the right-hand side of eq. (12b) is dominant due to a large σ_0 . As a result, we have $\sigma \approx \sigma_0 \exp(-\alpha_\sigma N)$ with $\alpha_\sigma \equiv m_\sigma^2/(3H^2)$. As we focus on the case where $\alpha_\sigma \ll 1$, the evolution of σ should be slow. Meanwhile, the slow growth of ϕ in the regime $\sigma \gtrsim \sigma_c$ indicates the presence of a stable fixed point of eq. (12a), where the classical drift and quantum diffusion compensate with each other. More specifically, we have

$$f(\langle \phi^2 \rangle, \sigma) \equiv C_1 \langle \phi^2 \rangle + C_2 \langle \phi^2 \rangle^2 - \frac{3H^4}{8\pi^2} = 0. \quad (15)$$

According to the bifurcation theory of differential equations, the critical condition at which the fixed point

ceases to be stable is given by $\partial f(\langle \phi^2 \rangle, \sigma)/\partial \langle \phi^2 \rangle = 0$, which yields the following equation for $\langle \phi^2 \rangle$

$$\langle \phi^2 \rangle = -\frac{C_1}{2C_2}. \quad (16)$$

Substituting eq. (16) into eq. (15), we arrive at the value of σ_t at the turning point as

$$\frac{\sigma_t}{\sigma_c} = \left(1 + \frac{B_p}{m_\phi^2} \right)^{\frac{1}{4}}, \quad (17)$$

with

$$B_3 = \left(\frac{9\Lambda^{16}}{2\pi^2\mu^6 M_{\text{Pl}}^4} \right)^{\frac{1}{3}}, \quad B_4 = \frac{\sqrt{2}\Lambda^6}{\pi\mu^2 M_{\text{Pl}}^2}. \quad (18)$$

In *quartic* hilltop inflation, with the help of eq. (17), we find that for the parameter values used in Fig. 2, the transition emerges at $\sigma_t \approx 1.1\sigma_c$, in excellent agreement with the numerical result. A similar consistency can also be observed in the case of *cubic* hilltop model.

After the turning point, ϕ grows rapidly, while the term proportional to $-\langle \phi^2 \rangle \langle \sigma^4 \rangle$ in eq. (12b) further drives σ downward. As a result, the value of σ at the exit from the diffusion region is slightly smaller than σ_t .

Eq. (17) predicts a characteristic value for the exit of ϕ from the diffusion region that is only weakly sensitive to the initial field values, apart from the unavoidable stochasticity induced by quantum fluctuations, provided that $\sigma_0 \gtrsim \sigma_t$ and $\phi_0 \approx 0$. Different pre-inflationary histories are driven into a relatively narrow onset window for hilltop inflation, which makes the corresponding initial condition considerably less fine-tuned. Moreover, as indicated by the numerical Langevin evolution, the actual value of σ when the system exits the diffusion region is typically slightly smaller than the estimate σ_t obtained from eq. (17). We therefore parametrize the effectively frozen curvaton field value during the subsequent hilltop inflationary stage as $\sigma_{\text{inf}} \simeq \xi \sigma_t$, with ξ being an $\mathcal{O}(1)$ factor slightly smaller than unity. Throughout the analysis we set $\xi = 0.75$, as motivated by our numerical results for the Langevin trajectories. We have further checked that the fit to the inflationary observables is not sensitive to small changes in ξ .

IV. PREDICTIONS FOR INFLATIONARY OBSERVABLES

A. Single-field slow-roll inflation

In the inflationary picture, quantum vacuum fluctuations on sub-horizon scales induce small anisotropies in the otherwise homogeneous background. During inflation, the comoving Hubble radius $\sim 1/(aH)$ (with a being the scale factor) decreases and eventually becomes smaller than the comoving wavelength of a given mode.

As a result, the quantum fluctuations are stretched to super-horizon scales and become effectively frozen until the end of inflation. For a mode with comoving wave number k , its perturbations after horizon exit can be described by a classical probability distribution, whose statistical properties are determined by the power spectrum evaluated at horizon crossing $k = aH$. In the single-field inflationary scenario, the power spectrum for scalar perturbations can be expressed as

$$\mathcal{P}_\zeta^{\text{inf}} = \frac{H^2}{4\pi^2} \frac{H^2}{\dot{\phi}^2} \Big|_{k=aH}, \quad (19)$$

which relates to the primordial curvature perturbations. For tensor perturbations, we have

$$\mathcal{P}_\mathcal{T}^{\text{inf}} = \frac{2}{\pi^2} \frac{H^2}{M_{\text{Pl}}^2} \Big|_{k=aH}. \quad (20)$$

By convention, the primordial power spectra are usually parametrized as power laws, namely,

$$\mathcal{P}_\zeta^{\text{inf}}(k) = A_s \left(\frac{k}{k_*} \right)^{n_s - 1 + \dots}, \quad (21a)$$

$$\mathcal{P}_\mathcal{T}^{\text{inf}}(k) = r A_s \left(\frac{k}{k_*} \right)^{n_t + \dots}, \quad (21b)$$

where k_* is a chosen pivot scale, A_s denotes the amplitude at k_* , $n_s \equiv 1 + d \ln \mathcal{P}_\zeta^{\text{inf}} / d \ln k$ refers to the spectral index, r represents the tensor-to-scalar ratio, and n_t is the tensor tilt.

The observational results from Planck [2], ACT [8], and BICEP/Keck [52] indicate that the scalar spectrum is nearly scale-invariant with a mild red tilt, and the tensor-to-scalar ratio is sufficiently close to zero. This supports the picture that the primordial fluctuations may be generated during a slow-roll inflationary epoch. One can define the following parameters

$$\epsilon \equiv \frac{M_{\text{Pl}}^2}{2} \left(\frac{V_\phi}{V} \right)^2, \quad \eta \equiv M_{\text{Pl}}^2 \frac{V_{\phi\phi}}{V}, \quad (22)$$

where $V_{\phi\phi} \equiv \partial^2 V / \partial \phi^2$. Then the slow-roll conditions turn out to be $\epsilon \ll 1$ and $|\eta| \ll 1$. In this case, the inflationary observables can be derived as

$$r \approx 16\epsilon_*, \quad n_s - 1 \approx 2\eta_* - 6\epsilon_*, \quad A_s \approx \frac{1}{24\pi^2 M_{\text{Pl}}^4} \frac{V}{\epsilon_*}, \quad (23)$$

where ϵ_* and η_* are calculated at k_* . Meanwhile, the number of e-folds $N_e \equiv \log(a_e/a_*)$ from the time when the k_* mode exits the horizon to the end of inflation can be computed as

$$N_e = \frac{1}{M_{\text{Pl}}^2} \int_{\phi_e}^{\phi_*} \frac{V}{V_\phi} d\phi, \quad (24)$$

where ϕ_e denotes the value of ϕ at which either ϵ or $|\eta|$ becomes greater than one. For the typical CMB pivot

scale $k_* = 0.05 \text{ Mpc}^{-1}$, we have $N_e \simeq 50 - 60$, depending on the post-inflationary reheating history. Hereafter, we take $N_e = 55$ for definiteness unless specified otherwise.

In the *quadratic* hilltop inflation model with $p = 2$, the slow-roll parameter $|\eta| = 2M_{\text{Pl}}^2/\mu^2$ is independent of ϕ . The slow-roll condition $|\eta| \ll 1$ therefore requires $\mu \gtrsim M_{\text{Pl}}$, implying that the inflaton field excursion is necessarily trans-Planckian. For $p > 2$ with sub-Planckian excursion, the slow-roll inflation terminates when $|\eta| \simeq 1$, corresponding to a field value ϕ_e satisfying

$$p(p-1)\phi_e^{p-2} \simeq \mu^p / M_{\text{Pl}}^2, \quad (25)$$

and the number of e-folds N_e during inflation can be approximated as

$$N_e \approx \frac{\mu^p}{p(p-2)M_{\text{Pl}}^2} \phi_*^{2-p}. \quad (26)$$

For a given N_e , this yields

$$\epsilon_* \propto \left(\frac{1}{N_e} \right)^{\frac{2p-2}{p-2}} \left(\frac{\mu}{M_{\text{Pl}}} \right)^{\frac{2p}{p-2}}, \quad (27)$$

indicating that $r \approx 16\epsilon_*$ is negligibly small. Meanwhile,

$$n_s \approx 1 - \frac{2(p-1)}{p-2} \frac{1}{N_e}, \quad (28)$$

which leads to $n_s \approx 0.927$ and 0.945 (assuming $N_e = 55$) for the *cubic* and *quartic* hilltop models, respectively, both of which lie outside the 95% C.L. regions in the latest Planck [2] and ACT [8] results.

B. The curvaton mechanism

The above picture can change if we introduce a curvaton field σ [37–41]. Since $m_\sigma \ll H$ during inflation, the curvaton is effectively frozen at σ_{inf} . Its quantum fluctuations at the horizon exit are promoted to classical perturbations with a nearly flat spectrum. At this stage, however, its contribution to the total curvature perturbations is negligible because of its tiny energy density, $\rho_\sigma \simeq m_\sigma^2 \sigma_{\text{inf}}^2 / 2$.¹ After inflation ends, the Hubble parameter H decreases as the Universe expands. When $H^2(t_{\text{osc}}) \equiv H_{\text{osc}}^2 \simeq m_\sigma^2$, which gives $T_{\text{osc}} \simeq \sqrt{m_\sigma M_{\text{Pl}}}$, the curvaton starts oscillating around its minimum and behaves as non-relativistic matter with an isocurvature density perturbation. Using the condition $H_{\text{osc}}^2 \simeq m_\sigma^2$, we have $\rho_r(t_{\text{osc}}) \simeq 3m_\sigma^2 M_{\text{Pl}}^2$. Since $\sigma_{\text{inf}} \ll M_{\text{Pl}}$, we see

¹ In the presence of the $\lambda^2 \phi^2 \sigma^4 / M_{\text{Pl}}^2$ term, the curvaton field does not behave purely as non-relativistic matter. A sizable σ^4 term would delay the epoch at which ρ_σ becomes dominant. In our numerical calculations, we have checked that at the end of inflation, when $\phi = \phi_e$, the curvaton energy density is indeed much smaller than the total energy density.

that at the oscillation time t_{osc} , the ratio of the curvaton energy density to the radiation energy density satisfies $(\rho_\sigma/\rho_r)|_{t_{\text{osc}}} \simeq (\sigma_{\text{inf}}/M_{\text{Pl}})^2/6 \ll 1$.

However, as $\rho_\sigma \propto a^{-3}$ while $\rho_r \propto a^{-4}$, the curvaton energy density becomes significant after sufficiently many Hubble times, provided that the oscillations last long enough before the curvaton decays. The final curvature perturbations then depend on the ratio between the curvaton energy density and the radiation energy density at the curvaton decay time t_{dec} defined as

$$R \equiv \left. \frac{\rho_\sigma}{\rho_r} \right|_{t_{\text{dec}}} \simeq \frac{1}{6} \left(\frac{\sigma_{\text{inf}}}{M_{\text{Pl}}} \right)^2 \left(\frac{T_{\text{osc}}}{T_{\text{dec}}} \right), \quad (29)$$

where T_{dec} denotes the curvaton decay temperature, which depends on the decay rate of the curvaton Γ_{curv} through $\Gamma_{\text{curv}} \simeq H(T_{\text{dec}})$. We can in turn get

$$\Gamma_{\text{curv}}^2 \simeq \frac{(1+R)\rho_r(T_{\text{dec}})}{3M_{\text{Pl}}^2} \approx \frac{m_\sigma^2 \sigma_{\text{inf}}^2}{6M_{\text{Pl}}^2} \left(\frac{T_{\text{dec}}}{T_{\text{osc}}} \right)^3, \quad (30)$$

where in the second step we have assumed that $R \gg 1$ so that the curvaton gives rise to large modifications to primordial observables in our model. With the help of eq. (30), T_{dec} can be written as

$$T_{\text{dec}} \simeq 2\sqrt{m_\sigma M_{\text{Pl}}} \left(\frac{M_{\text{Pl}}}{\sigma_{\text{inf}}} \right)^{\frac{2}{3}} \left(\frac{\Gamma_{\text{curv}}}{m_\sigma} \right)^{\frac{2}{3}}. \quad (31)$$

Meanwhile, using eqs. (29) and (30), we can estimate the magnitude of Γ_{curv} in the large R regime, namely,

$$\frac{\Gamma_{\text{curv}}}{m_\sigma} \simeq 6 \times 10^{-24} \left(\frac{\sigma_{\text{inf}}}{10^{14} \text{ GeV}} \right)^4 \left(\frac{500}{R} \right)^{\frac{3}{2}}. \quad (32)$$

Substituting this back into T_{dec} , we obtain

$$T_{\text{dec}} \simeq 1 \text{ GeV} \left(\frac{\sigma_{\text{inf}}}{10^{14} \text{ GeV}} \right)^2 \left(\frac{500}{R} \right) \left(\frac{m_\sigma}{10^6 \text{ GeV}} \right)^{\frac{1}{2}}. \quad (33)$$

Assuming an instant energy transfer from the curvaton to radiation, we obtain a temperature after the decay $T_{\text{RH}} \sim R^{1/4} T_{\text{dec}}$. Taking $\sigma_{\text{inf}} \sim 10^{14} \text{ GeV}$, $R \sim 500$, and $m_\sigma \sim 10^6 \text{ GeV}$, we obtain $T_{\text{RH}} \sim \text{GeV}$, which is well above Big-Bang Nucleosynthesis (BBN) bound $T_{\text{RH}} \gtrsim 4 - 5 \text{ MeV}$. Apparently, the determination of R depends on Γ_{curv} , which is rather model-dependent. In this work, instead of considering specific curvaton decay models, we regard R as a free parameter for simplicity.

The total curvature perturbation ζ on super-horizon scales is conserved for purely adiabatic evolution. In our scenario, ζ_r and ζ_σ denote the component curvature perturbations of the radiation and curvaton fluids, respectively. In the flat gauge, they are given by

$$\zeta_r = -H\delta\rho_r/\dot{\rho}_r = \delta\rho_r/(4\rho_r), \quad (34a)$$

$$\zeta_\sigma = -H\delta\rho_\sigma/\dot{\rho}_\sigma = \delta\rho_\sigma/(3\rho_\sigma), \quad (34b)$$

where ζ_σ is evaluated after the curvaton has entered its pressureless oscillating phase. Before the curvaton decay,

ζ_r is inherited from the inflaton decay products. At early times, when the curvaton energy density is negligible, one has $\zeta \simeq \zeta_r$. As the curvaton energy fraction grows, however, ζ evolves due to the relative entropy perturbation between the two fluids. In the sudden-decay approximation, the total curvature perturbation after decay is therefore written as [38]

$$\zeta = \frac{4\zeta_r + 3R\zeta_\sigma}{4 + 3R} = (1 - r_{\text{dec}})\zeta_r + r_{\text{dec}}\zeta_\sigma, \quad (35)$$

where $r_{\text{dec}} \equiv 3R/(4 + 3R)$. Unlike the standard curvaton mechanism, what we consider here is a mixed inflaton–curvaton scenario in which ζ_r can not be neglected [53–55]. It is convenient to rewrite eq. (35) as

$$\zeta = \zeta_r + r_{\text{dec}}(\zeta_\sigma - \zeta_r), \quad (36)$$

so that the adiabatic mode induced by the inflaton is carried by ζ_r , while the curvaton provides an additional contribution through the relative isocurvature perturbation $\zeta_\sigma - \zeta_r$. Accordingly, we define $\zeta_{\text{inf}} \equiv \zeta_r$ and $\zeta_{\text{curv}} \equiv r_{\text{dec}}(\zeta_\sigma - \zeta_r)$. Then the curvature perturbation power spectrum can be expressed as

$$\begin{aligned} \mathcal{P}_\zeta &= \mathcal{P}_\zeta^{\text{inf}} + \mathcal{P}_\zeta^{\text{curv}} + \mathcal{P}_\zeta^{\text{mix}} \\ &\propto \langle \zeta_{\text{inf}} \zeta_{\text{inf}} \rangle + \langle \zeta_{\text{curv}} \zeta_{\text{curv}} \rangle + 2\langle \zeta_{\text{inf}} \zeta_{\text{curv}} \rangle, \end{aligned} \quad (37)$$

where $\langle \dots \rangle$ denotes the correlation function.² In the flat gauge, the last term in eq. (37) is proportional to $\langle \delta\phi\delta\sigma \rangle$. Since the mass mixing between $\delta\phi$ and $\delta\sigma$ is proportional to λ^2 , $\langle \zeta_{\text{inf}} \zeta_{\text{curv}} \rangle$ should be negligibly small compared with the diagonal terms. Therefore, we can ignore the cross term,³ which results in $\mathcal{P}_\zeta \approx \mathcal{P}_\zeta^{\text{inf}} + \mathcal{P}_\zeta^{\text{curv}}$ with

$$\mathcal{P}_\zeta^{\text{inf}} = \left(\frac{H_*}{2\pi} \right)^2 \frac{1}{2\epsilon_* M_{\text{Pl}}^2}, \quad (38a)$$

$$\mathcal{P}_\zeta^{\text{curv}} = \left(\frac{R}{4 + 3R} \right)^2 \left(\frac{H_*}{\pi\sigma_{\text{inf}}} \right)^2. \quad (38b)$$

Evaluating the above quantities at the pivot CMB scale k_* gives the amplitudes

$$A_s^{\text{inf}} \equiv \mathcal{P}_\zeta^{\text{inf}}(k_*), \quad A_s^{\text{curv}} \equiv \mathcal{P}_\zeta^{\text{curv}}(k_*). \quad (39)$$

The total amplitude is $A_s = A_s^{\text{inf}} + A_s^{\text{curv}}$. Above, we see that the total curvature perturbations have different contributions from the inflaton and the curvaton, both depending on the ratio R .

² By definition, $\langle \zeta_{\mathbf{k}} \zeta_{\mathbf{k}'}^* \rangle = (2\pi)^3 \delta^{(3)}(\mathbf{k} - \mathbf{k}') P_\zeta(k)$. After horizon exit, each mode freezes and becomes effectively classical, so the power spectrum is given by the squared amplitude of the mode function at horizon exit $P_\zeta(k) = |\zeta_k^{\text{exit}}|^2$. Then the dimensionless power spectrum is given by $\mathcal{P}_\zeta(k) = k^3 P_\zeta(k)/(2\pi^2)$.

³ A more explicit form of the cross term is given in appendix B.

With the help of eqs. (38a) and (38b), we can derive the spectral index n_s as

$$\begin{aligned} n_s - 1 &= \frac{1}{\mathcal{P}_\zeta} \left(\frac{d\mathcal{P}_\zeta^{\text{inf}}}{d \ln k} + \frac{d\mathcal{P}_\zeta^{\text{curv}}}{d \ln k} \right) \Big|_{k_*} \\ &= \frac{A_s^{\text{inf}}}{A_s} (n_s^{\text{inf}} - 1) + \frac{A_s^{\text{curv}}}{A_s} (n_s^{\text{curv}} - 1), \end{aligned} \quad (40)$$

where n_s^{inf} can be calculated using eq. (23) in the slow-roll regime, whereas n_s^{curv} is given by [38]

$$n_s^{\text{curv}} - 1 \approx 2 \frac{\dot{H}_*}{H_*^2} + \frac{2}{3} \frac{m_\sigma^2}{H_*^2}. \quad (41)$$

In the case where $m_\sigma \ll H_*$ and $\dot{H}_*/H_*^2 \ll 1$, we approximately have $n_s^{\text{curv}} \approx 1$. We can now readily see how the presence of the curvaton modifies the inflationary predictions of hilltop models. In the single-field hilltop scenario, the amplitude of the primordial scalar spectrum A_s^{inf} can be compatible with observations, while the predicted spectral index n_s typically comes out too small in the sub-Planckian case. With the curvaton, both A_s and n_s are altered. The total amplitude A_s no longer needs to be entirely sourced by A_s^{inf} . Accordingly, one has $A_s^{\text{inf}}/A_s < 1$ in eq. (40), which implies $|n_s - 1| < |n_s^{\text{inf}} - 1|$, so that the predicted n_s can be closer to unity compared to the single-field hilltop case. Using the best-fit values $n_s = 0.9649$ and $\ln(10^{-10} A_s) = 3.049$ from Planck18 (TT,TE,EE+lowE) results for illustration, one arrives at $A_s^{\text{inf}} \simeq 1.0 \times 10^{-9}$ and $A_s^{\text{curv}} \simeq 1.1 \times 10^{-9}$ for the *cubic* hilltop, and $A_s^{\text{inf}} \simeq 1.3 \times 10^{-9}$ and $A_s^{\text{curv}} \simeq 7.6 \times 10^{-10}$ for the *quartic* hilltop.

In addition, the tensor-to-scalar ratio r also gets modified, i.e.,

$$r = \frac{A_t}{A_s} = \frac{16\epsilon_*}{1 + A_s^{\text{curv}}/A_s^{\text{inf}}}, \quad (42)$$

where $A_t = 2H_*^2/(\pi^2 M_{\text{Pl}}^2)$ has been adopted.

In appendix B, we re-derive the above results adopting the δN formalism [56, 57]. Moreover, the δN formalism could also help us calculate the magnitude of the primordial non-Gaussianity [57–60], which may be significant in the curvaton scenario, since the final curvature perturbations arise from the nonlinear conversion of the curvaton isocurvature fluctuations into adiabatic ones after its decay. The local non-Gaussianity can be described by a dimensionless parameter f_{NL} , which can be estimated as [cf. eq. (B15)]

$$f_{\text{NL}} \approx \left(\frac{A_s^{\text{curv}}}{A_s} \right)^2 \left(\frac{5}{4r_{\text{dec}}} - \frac{5}{3} - \frac{5}{6} r_{\text{dec}} \right). \quad (43)$$

V. RESULTS AND DISCUSSIONS

In this section, we test the curvaton-assisted *cubic* and *quartic* hilltop inflation models against the CMB observations. Before proceeding to the numerical analysis, we shall make some analytical order-of-magnitude estimates.

We focus on the scenario where the primary inflationary phase can be approximately described by a purely *cubic* or *quartic* hilltop potential, for which the formulae for the primordial observables remain valid. To achieve this, we require $B_p \lesssim m_\phi^2$, so that V_ϕ is dominated by the second term in eq. (8). By adopting the formulae in single-field slow-roll hilltop inflation, we can rewrite eqs. (38a) and (38b) as the expressions that depend explicitly on the model parameters. For A_s^{inf} , we have

$$A_s^{\text{inf}} \approx \frac{3N_e^4 M_{\text{Pl}}^2 \Lambda^4}{4\pi^2 \mu^6} \quad (\text{cubic hilltop}), \quad (44a)$$

$$A_s^{\text{inf}} \approx \frac{8N_e^3 \Lambda^4}{3\pi^2 \mu^4} \quad (\text{quartic hilltop}), \quad (44b)$$

and

$$A_s^{\text{curv}} \approx \frac{\lambda \Lambda^4}{27\pi^2 m_\phi M_{\text{Pl}}^3}. \quad (45)$$

where we have assumed $R \gg 1$ and omitted the $\mathcal{O}(1)$ factor ξ . It can be seen that Λ exhibits a positive relation with μ , whereas it shows a negative relation with λ . The ratio between A_s^{inf} and A_s^{curv} turns out to be

$$\frac{A_s^{\text{inf}}}{A_s^{\text{curv}}} = \frac{81N_e^4 m_\phi M_{\text{Pl}}^5}{4\lambda \mu^6} \quad \text{and} \quad \frac{72N_e^3 m_\phi M_{\text{Pl}}^3}{\lambda \mu^4}, \quad (46)$$

for the *cubic* and *quartic* hilltop models, respectively. Λ approximately cancels out in the ratio. One can thus see from eqs. (40) and (42) that the dependence of n_s and r on Λ is weak. In addition, we should require that $|V_{\sigma\sigma}| = m_\sigma^2 + 6\lambda^2 \phi^2 \sigma_{\text{inf}}^2 / M_{\text{Pl}}^2 \lesssim H^2$ holds at ϕ_e , which turns out to be a strong constraint on the parameter space. More accurately, one can see from eq. (25) that $\phi_e^2 \simeq \mu^6 / (36M_{\text{Pl}}^4)$ in the *cubic* case and $\phi_e^2 \simeq \mu^4 / (12M_{\text{Pl}}^2)$ in the *quartic* case. After substituting the analytical estimate of ϕ_e into eq. (46), we find that the *cubic* case carries one extra power of N_e in $A_s^{\text{inf}}/A_s^{\text{curv}}$, compared with the *quartic* case. As a result, demanding A_s^{inf} and A_s^{curv} to be of comparable size typically pushes the *cubic* model towards a larger ϕ_e , which makes the condition $|V_{\sigma\sigma}| \lesssim H^2$ much harder to satisfy.

Based on the above discussions, we perform an illustrative Bayesian analysis to assess the consistency of our curvaton-assisted hilltop inflation model with cosmological observations. We fix the values of $m_\phi = 3 \times 10^{-11} M_{\text{Pl}}$, $m_\sigma = 5 \times 10^{-12} M_{\text{Pl}}$, and $R = 500$,⁴ while treating the

⁴ The choice of fixing the values of $\{R, m_\phi, m_\sigma\}$ is motivated as follows. First, from eq. (38b), a sizable curvaton contribution to the scalar power spectrum requires a sufficiently large R , while for $R \gg 1$ the prefactor $R/(4+3R)$ is already close to saturation and depends only weakly on the precise value of R . Second, m_ϕ affects A_s^{curv} mainly through the value of $\sigma_{\text{inf}} \simeq \xi \sigma_t$ at the exit from the diffusion region. On the one hand, according to eq. (38b), obtaining a sizable A_s^{curv} disfavors very large m_ϕ . On

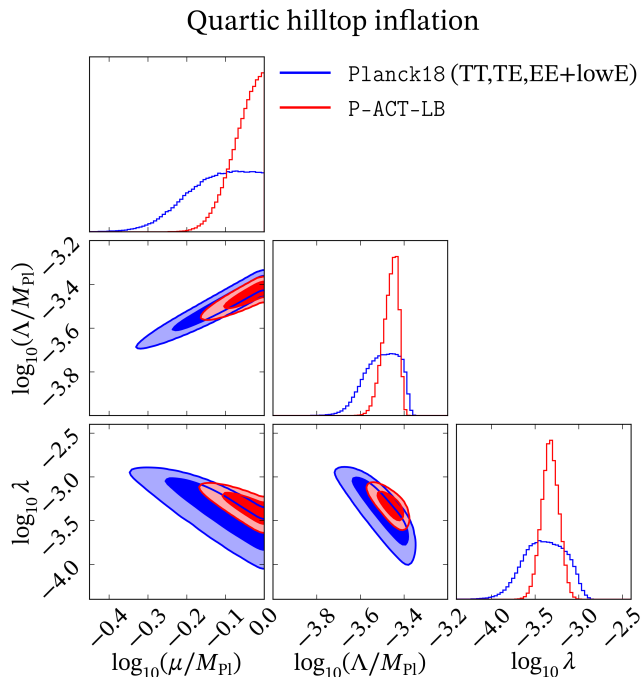


FIG. 3: The 1D marginalized and 2D joint posterior probability distributions for the model parameters $\{\mu, \Lambda, \lambda\}$ in the *quartic* hilltop model, where we fix $R = 500$, $m_\phi = 3 \times 10^{-11} M_{\text{Pl}}$, and $m_\sigma = 5 \times 10^{-12} M_{\text{Pl}}$. Constraints are derived from an MCMC Bayesian analysis incorporating observational data for n_s and \mathcal{A}_s from **Planck18** (TT,TE,EE+lowE) (blue) and **P-ACT-LB** (red), as well as the upper limit on the tensor-to-scalar ratio $r < 0.036$ at 95% C.L. from **BICEP/Keck18** (BK18). The inner and outer contours in the 2D plots correspond to the 68% and 95% credible intervals, respectively.

remaining parameters $\theta = \{\mu, \Lambda, \lambda\}$ as the scanning parameters. A log-flat (uniform-in-log) prior is imposed on these parameters, such that $\pi(\theta) = 1$ for

$$\begin{aligned} -1 \leq \log_{10}(\mu/M_{\text{Pl}}) \leq 0, \quad -5 \leq \log_{10}(\Lambda/M_{\text{Pl}}) \leq -2, \\ -5 \leq \log_{10} \lambda \leq -1, \quad (|V_{\sigma\sigma}/H^2)|_{\phi_e} < 1. \end{aligned} \quad (47)$$

Otherwise, $\pi(\theta) = 0$. Here we restrict the prior range to $\mu \lesssim M_{\text{Pl}}$ to maintain a clean separation between the sub-Planckian and trans-Planckian regimes. However, we note that this is mainly a choice for definiteness. In hilltop inflation, even when μ is slightly larger than M_{Pl} , e.g. $\mu \simeq 2M_{\text{Pl}}$, the actual inflaton excursion may still remain below the Planck scale.

the other hand, as shown in appendix C, once $m_\phi^2 \ll B_3$, σ_t becomes nearly independent of m_ϕ . We therefore fix m_ϕ to a representative value. Finally, the role of m_σ is mainly to ensure that the curvaton remains effectively frozen during hilltop inflation, and its impact on the inflationary observables is negligible within the parameter region of interest.

TABLE I: Marginalized posterior constraints for the curvaton assisted *quartic* hilltop model in the sub-Planckian region, where we set $R = 500$, $m_\phi = 3 \times 10^{-11} M_{\text{Pl}}$ and $m_\sigma = 5 \times 10^{-12} M_{\text{Pl}}$. Unless otherwise stated, quoted uncertainties correspond to the marginalized 68% credible intervals. For μ in the P-ACT-LB case, we quote the 95% lower bound, since its posterior is visibly skewed toward the prior boundary $\mu < M_{\text{Pl}}$. For r , we quote the 95% upper bound.

Parameters	<i>Quartic</i> hilltop	
	Planck18	P-ACT-LB
$\log_{10}(\mu/M_{\text{Pl}})$	$-0.113^{+0.077}_{-0.093}$	> -0.129
μ/M_{Pl}	$0.771^{+0.149}_{-0.149}$	> 0.743
$\log_{10}(\Lambda/M_{\text{Pl}})$	$-3.497^{+0.075}_{-0.086}$	$-3.457^{+0.029}_{-0.041}$
Λ/M_{Pl}	$(3.18^{+0.60}_{-0.57}) \times 10^{-4}$	$(3.49^{+0.24}_{-0.32}) \times 10^{-4}$
$\log_{10} \lambda$	$-3.386^{+0.244}_{-0.243}$	$-3.326^{+0.099}_{-0.098}$
λ	$(4.11^{+3.09}_{-1.76}) \times 10^{-4}$	$(4.72^{+1.21}_{-0.95}) \times 10^{-4}$
n_s	$0.9630^{+0.0041}_{-0.0043}$	$0.9720^{+0.0025}_{-0.0029}$
\mathcal{A}_s	$3.045^{+0.016}_{-0.016}$	$3.060^{+0.011}_{-0.011}$
r	$< 10^{-6}$	$< 10^{-6}$
f_{NL}	$-0.114^{+0.053}_{-0.066}$	$-0.278^{+0.060}_{-0.058}$

For the purpose of a phenomenological estimate, we construct a simplified likelihood in terms of the observables $D = \{\mathcal{A}_s, n_s, r\}$ (with $\mathcal{A}_s \equiv \ln(10^{10} A_s)$). For simplicity, we assume the measurement errors are Gaussian and uncorrelated, and then the log-likelihood is related to the χ^2 statistic as $\log \mathcal{L} = -\chi^2/2$, where the total χ^2 is calculated as the sum of the contributions from each observable

$$\chi^2(\theta) = \frac{(n_s(\theta) - \bar{n}_s)^2}{\sigma_{n_s}^2} + \frac{(\mathcal{A}_s(\theta) - \bar{\mathcal{A}}_s)^2}{\sigma_{\mathcal{A}_s}^2} + \frac{r^2(\theta)}{\sigma_r^2}, \quad (48)$$

where $n_s(\theta)$, $\mathcal{A}_s(\theta)$, and $r(\theta)$ are the values predicted by the model for the parameter set θ , the values \bar{n}_s and $\bar{\mathcal{A}}_s$ are the observed central values, and σ represents the corresponding 1σ (68% C.L.) uncertainties. This simplified likelihood is sufficient for identifying viable benchmark regions, but should not be regarded as a substitute for a full experimental likelihood analysis. As discussed above, we adopt the **Planck18** (TT,TE,EE+lowE) constraints and the combination of ACT DR6, Planck, and DESI Year-1 data, labeled by **P-ACT-LB** as the observational baselines for our parameter inference. For **Planck18** (TT,TE,EE+lowE), the central values and the corresponding 68% C.L. uncertainties for n_s and \mathcal{A}_s at the pivot $k_* = 0.05 \text{ Mpc}^{-1}$ are determined by [2]

$$n_s = 0.9649 \pm 0.0044, \quad \mathcal{A}_s = 3.045 \pm 0.016, \quad (49)$$

while for P-ACT-LB, we use⁵ [8]

$$n_s = 0.9743 \pm 0.0034, \quad \mathcal{A}_s = 3.060_{-0.012}^{+0.011}. \quad (50)$$

For the tensor-to-scalar ratio r , the most stringent upper bound is derived from the BICEP/Keck18 (BK18) result [52], namely,

$$r < 0.036 \text{ (95\% C.L.) at } k_* = 0.05 \text{ Mpc}^{-1}. \quad (51)$$

We thereby model the χ^2 function for r as a one-sided Gaussian distribution with a mean of zero and a standard deviation $\sigma_r = 0.036/1.96 = 0.0184$.

The posterior probability distribution $P(\theta|D)$ of the parameters θ given the observational data D is proportional to the product of the likelihood function $\mathcal{L}(D|\theta)$ and the prior probability distribution $\pi(\theta)$

$$P(\theta|D) \propto \mathcal{L}(D|\theta)\pi(\theta). \quad (52)$$

We explore the parameter space using an MCMC algorithm. For the *cubic* hilltop model, we do not find any viable parameter region with $\mu < M_{\text{Pl}}$ in our numerical scans, even after varying m_ϕ , m_σ and R . The main issue is that the model cannot simultaneously reproduce the observed inflationary observables and satisfy the curvaton condition. A detailed analysis of the viability of the *cubic* hilltop model can be found in appendix C. In contrast, in the *quartic* model we find a parameter region that is consistent with current cosmological observations. The resulting 1D and 2D marginalized posterior distributions are displayed as corner plots in Fig. 3. The inner and outer contours correspond to the 68% and 95% credible intervals (i.e., approximately 68% and 95% of the samples fall within the corresponding contours), while the blue and red shaded regions represent the constraints from the Planck18 and P-ACT-LB, respectively. Meanwhile, we also present marginalized posterior constraints for model parameters $\{\mu, \Lambda, \lambda\}$ and the predicted values of \mathcal{A}_s , n_s , r and f_{NL} in Table I. Some remarks are as follows.

Firstly, our analysis demonstrates that the curvaton-assisted *quartic* hilltop inflation model is consistent with current observations from both Planck and ACT collaborations. It is evident that P-ACT-LB yields more compact posterior distributions, providing more stringent constraints on the model parameters.

Secondly, the preferred value of Λ from the posterior distributions is around $\mathcal{O}(10^{15})$ GeV, implying a potential origin from Grand Unified Theories (GUTs). The median value of the coupling parameter λ is determined to be $\sim 4 \times 10^{-4}$. As for the parameter μ , the 1D posterior is skewed toward the upper prior boundary $\mu < M_{\text{Pl}}$. In the Planck18 case, the distribution already shows a

clear flattening before the imposed cutoff $\mu < M_{\text{Pl}}$ is reached, and still admits a meaningful 68% credible interval, $\mu/M_{\text{Pl}} = 0.771_{-0.149}^{+0.149}$. In contrast, the P-ACT-LB posterior is more strongly piled up against the boundary, with about 32% of the samples satisfying $\mu/M_{\text{Pl}} > 0.95$, indicating a substantial prior-boundary effect. For this reason, we quote the constraint on μ in terms of a one-sided 95% lower bound.

Finally, the parameter relations exhibited in the 2D posterior distributions indicate that μ is negatively correlated with λ and positively correlated with Λ , which are well described by the analytical formulae in eqs. (44a), (44b) and (45).

So far, our analysis has focused on the sub-Planckian hilltop regime. In that case, the inclusion of the curvaton alleviates the tension with observations, while the predicted tensor-to-scalar ratio remains negligible, $r < 10^{-6}$. It is nevertheless instructive to briefly examine the trans-Planckian regime with $\mu \gtrsim M_{\text{Pl}}$, where the inflationary dynamics is qualitatively different. In this case, the end of slow-roll inflation is no longer determined by $\eta = -1$, but instead by $\epsilon = 1$. Accordingly, the field value at the end of inflation, ϕ_e , is no longer given by eq. (25), and the corresponding $r - n_s$ relation is modified. For the hilltop potential $V(\phi) \propto 1 - (\phi/\mu)^p + \dots$, one obtains at first order in the slow-roll approximation [61]

$$r \approx \frac{8p^2(M_{\text{Pl}}/\mu)^2 x^{2p-2}}{(1-x^p)^2}, \quad (53a)$$

$$n_s - 1 \approx -\frac{2p(p-1)(M_{\text{Pl}}/\mu)^2 x^{p-2}}{1-x^p} - \frac{3r}{8}, \quad (53b)$$

where $x \equiv \phi_*/\mu$. In the limit $\mu \gg M_{\text{Pl}}$, this reduces to $n_s \approx 1 - 3r/8$.

The blue curves in Fig. 4 show the corresponding $r - n_s$ relations for the single-field *quartic* hilltop inflation model, together with the experimental constraints from P-ACT-LB-BK18 and Planck-LB-BK18. In this regime, r is significantly enhanced, leading to stronger tension with the data, especially once ACT data are included. Even for the $N_e = 60$ case, the theoretical prediction lies almost entirely outside the 68% credible region of the P-ACT-LB-BK18 constraints.

For comparison, we also illustrate the behavior of the curvaton-assisted model in the trans-Planckian regime. This part is intended only as an illustrative extension, rather than as a full Bayesian analysis analogous to the sub-Planckian case discussed above. As a representative example, we fix $\lambda = 10^{-6}$ and select points satisfying the basic observational requirement $3.0 < \mathcal{A}_s < 3.1$. The green curves in Fig. 4 are then obtained by averaging r within each n_s bin for these selected points. One sees that r is suppressed relative to the single-field case, giving typically $r \sim \mathcal{O}(0.01)$ for $n_s \sim 0.97$. This suggests that, unlike the single-field trans-Planckian hilltop model, the curvaton-assisted scenario can remain compatible with current constraints while predicting a potentially observable tensor signal, making it an interesting target for fu-

⁵ We approximate $\sigma_{\mathcal{A}_s}$ by the average value $\sigma_{\mathcal{A}_s} = 0.0115$ when constructing the likelihood function for \mathcal{A}_s .

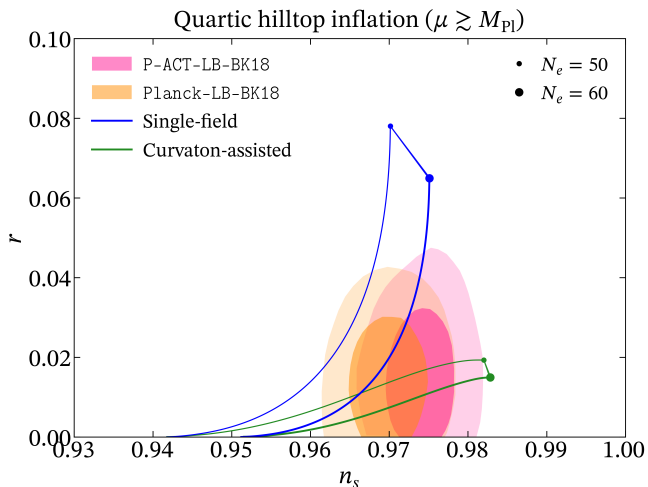


FIG. 4: Relations between the tensor-to-scalar ratio r and the spectral index n_s in the trans-Planckian *quartic* hilltop model where $\mu \gtrsim M_{\text{Pl}}$. The pink- and orange-shaded contours are the constraints from the P-ACT-LB-BK18 and Planck-LB-BK18 results, with the darker and lighter colors denoting the 68% and 95% C.L. allowed regions, respectively [64]. Blue lines correspond to the predicted $r - n_s$ relations in the single-field hilltop models, while the green lines represent the $r - n_s$ relations in the curvaton-assisted *quartic* hilltop model for $\lambda = 10^{-6}$, obtained from the viable points with \mathcal{A}_s restricted to the narrow range $3.0 < \mathcal{A}_s < 3.1$, by averaging r in each n_s bin. Note that here the results for the curvaton-assisted hilltop model are also derived within the trans-Planckian regime.

ture CMB experiments such as LiteBIRD [62] and CMB-S4 [63].

Before closing this section, we turn to a brief comment on the non-Gaussianity. According to Table I, the preferred local non-Gaussianity coefficient f_{NL} is found to be negative with a magnitude of $\mathcal{O}(0.1)$. The up-to-date constraint on the local non-Gaussianity is $f_{\text{NL}} = -0.9 \pm 5.1$ [3]. Hence our prediction for the non-Gaussianity lies well within current experimental limits, yet still represents a small but distinct deviation from the standard single-field slow-roll prediction $f_{\text{NL}} \sim \mathcal{O}(1 - n_s)$.

VI. CONCLUSIONS

Conventional hilltop inflation models face the initial-condition problem that the inflaton field must start to roll extremely close to the top of the hilltop potential, raising a concern about its naturalness. In this work, we have discussed a mechanism involving a curvaton field that significantly relaxes this problem. We have focused on the *cubic* and *quartic* hilltop models in particular. The curvaton σ couples to the inflaton field via a cross term given in eq. (5), which contributes to the effective mass

of the inflaton and modulates the shape of the inflaton potential. The required operators can be embedded in a supersymmetric framework.

Given white-noise fluctuations at the Hubble scale for both inflaton and curvaton fields, we have shown, both analytically and numerically, that the onset of hilltop inflation is insensitive to the initial position of the curvaton within a certain region of field space. The dynamics of the field evolution is described by the Langevin equations. In the numerical simulation, we applied an MCMC analysis to solve the equations, and in the analytical derivation, mean-square values of the fields ϕ and σ were taken as observables. Both results match very well, as shown in Fig. 1, and the insensitivity to the initial conditions is confirmed in Fig. 2.

The curvaton is assumed to be sufficiently light compared with the Hubble rate during inflation, so that it does not dominate the Universe until the Hubble rate decreases to become comparable to the curvaton mass after inflation. It plays an essential role in modifying the primordial curvature perturbations via the ratio R of the curvaton energy density to the radiation energy density at the time of curvaton decay. We have explicitly derived the expressions for the primordial observables in the presence of a curvaton.

We further performed an illustrative Bayesian analysis, based on a simplified likelihood constructed from the Planck and recent ACT results, to confirm the consistency of our model with cosmological observations. Given a sufficiently large R and suitable inflaton and curvaton masses, the overall potential scale Λ can be of order the GUT scale, and the inflaton field value can be of order the sub-Planckian scale, both remaining consistent with these data in the *quartic* hilltop model. Furthermore, we compared our model with single-field hilltop inflation in terms of the predicted tensor-to-scalar ratio and spectral index in the trans-Planckian regime. A tensor-to-scalar ratio of $\mathcal{O}(0.01)$ was obtained in the curvaton-assisted inflation scenario with $\mu \gg M_{\text{Pl}}$ and $\lambda = 10^{-6}$, consistent with both the Planck and the recent ACT data, and this can be tested in next-generation CMB experiments.

ACKNOWLEDGMENTS

We are grateful to Stefan Antusch for useful discussions. XW thanks Changyuan Yao for valuable discussions on coding. WA is supported by the European Union (ERC, NLO-DM, 101044443). SFK acknowledges the STFC Consolidated Grant ST/X000583/1 and thanks IFIC, Valencia, for hospitality; his work was funded by a Leverhulme Trust Emeritus Fellowship Grant. XW acknowledges the Royal Society as the funding source of the Newton International Fellowship; his work is partially funded by the European Union, NextGenerationEU, National Recovery and Resilience Plan (mission 4, component 2) under the project *MODIPAC: Modular Invariance in Particle Physics and Cosmology* (CUP

C93C24004940006). YLZ is partially supported by the National Natural Science Foundation of China (NSFC) under Grant Nos. 12535007, 12547104, and Zhejiang Provincial Natural Science Foundation of China under Grant No. LDQ24A050002.

Appendix A: Langevin Equations

In the stochastic inflation formalism, the evolution of the coarse-grained scalar field is governed by two contributions: a deterministic drift corresponding to its classical slow-roll motion, and a stochastic source arising from the continuous horizon crossing and subsequent freezing of short-wavelength quantum fluctuations. As a result, the dynamics of the field can be described by a stochastic differential equation of Langevin type [65]

$$d\varphi = -\frac{V_\varphi}{3H^2}dN + \frac{H}{2\pi}dW_N, \quad (\text{A1})$$

where $\varphi = \phi, \sigma$ and W_N denotes the Wiener stochastic process with increments satisfying $\langle dW_N \rangle = 0$ and $\langle (dW_N)^2 \rangle = dN$. dW_N is related to the white noise ξ_φ via $dW_N = \xi_\varphi dN$. Then one can immediately note that eq. (A1) takes the same form as eqs. (9) and (10).

Taking the expectation value of eq. (A1) and utilizing $\langle dW_N \rangle = 0$, we obtain the Langevin equation of the expectation value $\langle \varphi \rangle$ as

$$\frac{d\langle \varphi \rangle}{dN} = -\frac{\langle V_\varphi \rangle}{3H^2}. \quad (\text{A2})$$

In order to derive the Langevin equation for the field mean-square values, we consider the stochastic differential of φ^2 , namely,

$$\begin{aligned} d(\varphi^2) &= 2\varphi d\varphi + (d\varphi)^2 \\ &= -\varphi \frac{2V_\varphi}{3H^2}dN + 2\varphi \frac{H}{2\pi}dW_N + \left(\frac{H}{2\pi}\right)^2 dN, \end{aligned} \quad (\text{A3})$$

where $(d\varphi)^2$ cannot be neglected since $\langle (dW_N)^2 \rangle = dN$ is of first order in the infinitesimal. Again, taking the expectation value of eq. (A3) and using $\langle \varphi dW_N \rangle = 0$, we obtain Langevin equation for $\langle \varphi^2 \rangle$

$$\frac{d\langle \varphi^2 \rangle}{dN} = -\frac{2}{3H^2} \langle V_\varphi \cdot \varphi \rangle + \left(\frac{H}{2\pi}\right)^2. \quad (\text{A4})$$

For our model setup with $\lambda \lesssim 10^{-2}$, the covariance between ϕ and σ is negligible, which allows us to treat the Langevin equations for ϕ and σ separately. As mentioned in the main text, the starting point of σ is randomly selected in the range $\sigma \gtrsim \sigma_c$, while the initial value of ϕ is very close to zero. In this case, $V_\sigma \approx m_\sigma^2 \sigma$ and eq. (A4) reduces to

$$\frac{d\langle \sigma^2 \rangle}{dN} \approx -\frac{2m_\sigma^2}{3H^2} \langle \sigma^2 \rangle - \frac{4\lambda^2 \langle \phi^2 \rangle \langle \sigma^4 \rangle}{3H^2 M_{\text{Pl}}^2} + \left(\frac{H}{2\pi}\right)^2, \quad (\text{A5})$$

which reproduces eq. (12b). As for the field ϕ , since V_ϕ contains higher-order terms in ϕ , in general one cannot reduce the equation for $\langle \phi^2 \rangle$ into a form analogous to eq. (A5). In the following, we examine the explicit forms of Langevin equations for $\langle \phi^2 \rangle$ for the *cubic* and *quartic* hilltop cases.

Cubic hilltop. In the *cubic* hilltop case with $p = 3$, V_ϕ is written as

$$V_\phi = m_\phi^2 \left(\frac{\sigma^4}{\sigma_c^4} - 1 \right) \phi - 3\Lambda^4 \frac{\phi^2}{\mu^3} + \dots \quad (\text{A6})$$

From eq. (A2), it is not difficult to see that ϕ can develop a nonzero expectation value due to the ϕ^2 term in V_ϕ . A static solution can be reached if $d\langle \phi \rangle / dN \simeq 0$ is satisfied, which yields

$$\langle \phi \rangle \simeq \frac{3\Lambda^4 \langle \phi^2 \rangle}{m_\phi^2 \mu^3} \left(\frac{\sigma^4}{\sigma_c^4} - 1 \right)^{-1}. \quad (\text{A7})$$

For the parameter range of interest, $\langle \phi \rangle \lesssim \phi_{\text{rms}} \equiv \sqrt{\langle \phi^2 \rangle}$ holds. Hence, under the condition that ϕ follows an approximately Gaussian distribution, one can get $\langle \phi^3 \rangle \approx 3\langle \phi \rangle \cdot \langle \phi^2 \rangle$. Then eq. (A4) can be recast into

$$\frac{d\langle \phi^2 \rangle}{dN} \approx -\frac{2}{3H^2} (C_1 \langle \phi^2 \rangle + C_2 \langle \phi^2 \rangle^2) + \left(\frac{H}{2\pi}\right)^2, \quad (\text{A8})$$

with

$$C_1 = m_\phi^2 \left(\frac{\langle \sigma^4 \rangle}{\sigma_c^4} - 1 \right), \quad C_2 = -\frac{27\Lambda^8}{m_\phi^2 \mu^6} \left(\frac{\langle \sigma^4 \rangle}{\sigma_c^4} - 1 \right)^{-1}. \quad (\text{A9})$$

Quartic hilltop. Unlike the *cubic* hilltop potential, in the *quartic* hilltop case we have

$$V_\phi = m_\phi^2 \left(\frac{\sigma^4}{\sigma_c^4} - 1 \right) \phi - 4\Lambda^4 \frac{\phi^3}{\mu^4} + \dots, \quad (\text{A10})$$

which involves only odd powers of ϕ . Therefore, as long as $\langle \phi \rangle$ is sufficiently close to zero, it will eventually stabilize at $\langle \phi \rangle = 0$. For an approximate Gaussian distribution, $\langle \phi^4 \rangle = 3\langle \phi^2 \rangle^2$ should be satisfied. In this case, the Langevin equation for $\langle \phi^2 \rangle$ also takes the form as

$$\frac{d\langle \phi^2 \rangle}{dN} \approx -\frac{2}{3H^2} (C_1 \langle \phi^2 \rangle + C_2 \langle \phi^2 \rangle^2) + \left(\frac{H}{2\pi}\right)^2, \quad (\text{A11})$$

with

$$C_1 = m_\phi^2 \left(\frac{\langle \sigma^4 \rangle}{\sigma_c^4} - 1 \right), \quad C_2 = -\frac{12\Lambda^4}{\mu^4}. \quad (\text{A12})$$

Appendix B: δN formalism

In this section, we derive the explicit formulae for inflationary observables in our model by implementing the

δN formalism [56, 57, 66]. On super-horizon scales, the curvature perturbation ζ appears in the spatial part of the perturbed metric ds^2 in the form

$$ds^2 = -dt^2 + a^2(t)e^{2\zeta(t,\mathbf{x})}\delta_{ij}dx^i dx^j. \quad (\text{B1})$$

Accordingly, the physical volume element $dV(\mathbf{x})$ around the position \mathbf{x} is proportional to $a^3(t)e^{3\zeta(t,\mathbf{x})}$. On the other hand, the expansion of the background volume can be connected to the number of e-folds as $a^3(t) \sim e^{3N}$. As a result, $dV(\mathbf{x}) \propto e^{3[N+\delta N(\mathbf{x})]}$ with $\delta N(\mathbf{x})$ being the difference between the local number of e-folds in each Hubble patch and the background average. Hence one can directly identify the curvature perturbation with the local fluctuation in the number of e-folds, namely, $\zeta(\mathbf{x}) = \delta N(\mathbf{x})$.

In practice, one can select a spatially flat slice where the curvature perturbation in the three-dimensional metric vanishes as the initial hypersurface, labeled by “*”, and a uniform-density slice where $\delta\rho = 0$ as the final hypersurface, labeled by “f”. Note that the flat hypersurface must be evaluated at the horizon exit. Then we have $\zeta = \delta N_*^f$. In the two-field framework, δN_*^f can be computed with the help of Taylor expanding [66]

$$\delta N_*^f = N_i \delta\varphi_*^i + \frac{1}{2} N_{ij} \delta\varphi_*^i \delta\varphi_*^j + \dots, \quad (\text{B2})$$

with $N_i \equiv \partial N_*^f / \partial\varphi_*^i$, $N_{ij} \equiv \partial^2 N_*^f / (\partial\varphi_*^i \partial\varphi_*^j)$, and $\varphi = \phi, \sigma$ in our case. We adopt the sudden-decay approximation for the curvaton and take the final uniform-density hypersurface to coincide with the epoch of its decay, and then N_ϕ and N_σ can be evaluated by

$$N_\phi = \frac{1}{M_{\text{Pl}}\sqrt{2\epsilon_*}}, \quad N_\sigma = \frac{2r_{\text{dec}}}{3\sigma_{\text{inf}}}. \quad (\text{B3})$$

where

$$r_{\text{dec}} \equiv \left. \frac{3\rho_\sigma}{4\rho_r + 3\rho_\sigma} \right|_{\text{decay}}. \quad (\text{B4})$$

The factor r_{dec} enters the expressions for N_ϕ and N_σ because, after the curvaton decay, the total curvature perturbation ζ is a weighted combination of the adiabatic and isocurvature contributions, namely, $\zeta = \zeta_r + r_{\text{dec}}(\zeta_\sigma - \zeta_r)$.

Now we can use the above formulae to calculate corresponding inflationary observables.

Power spectrum. The total power spectrum reads

$$\begin{aligned} \mathcal{P}_\zeta &\equiv \langle \zeta\zeta \rangle = N_i N_j \langle \delta\varphi_*^i \delta\varphi_*^j \rangle \\ &= \left(\frac{H_*}{2\pi} \right)^2 (N_\phi^2 + N_\sigma^2 + 2\kappa N_\phi N_\sigma), \end{aligned} \quad (\text{B5})$$

where the coefficient $\kappa \equiv \langle \delta\phi_* \delta\sigma_{\text{inf}} \rangle / [H_*^2 / (2\pi)^2]$. Under the assumption that σ is light and the mixing between ϕ and σ is weak, $\kappa \sim M_{\text{Pl}}^2 V_{\phi\sigma} / V = 4\lambda^2 \phi \sigma^3 / V \ll 1$ can be safely neglected. Hence we get

$$\mathcal{P}_\zeta \approx \left(\frac{H_*}{2\pi} \right)^2 \left[\frac{1}{2\epsilon_* M_{\text{Pl}}^2} + \left(\frac{2r_{\text{dec}}}{3\sigma_{\text{inf}}} \right)^2 \right], \quad (\text{B6})$$

which turns out to be eqs. (38a) and (38b).

Tensor-to-scalar ratio. As the introduction of the curvaton only modifies the scalar perturbation power spectrum, the tensor-to-scalar ratio becomes

$$r \equiv \frac{\mathcal{P}_\mathcal{T}}{\mathcal{P}_\zeta} = \frac{8}{M_{\text{Pl}}^2 (N_\phi^2 + N_\sigma^2)}. \quad (\text{B7})$$

Substituting eq. (B3) into the above equation, we obtain

$$r = \frac{16\epsilon_*}{1 + 2\epsilon_* M_{\text{Pl}}^2 [2r_{\text{dec}} / (3\sigma_{\text{inf}})]^2}. \quad (\text{B8})$$

Spectral index. In the δN formalism, the spectral index can be expressed as

$$\begin{aligned} n_s &= 1 + \frac{N_\phi^2}{N_\phi^2 + N_\sigma^2} (-6\epsilon_* + 2\eta_*) \\ &\quad + \frac{N_\sigma^2}{N_\phi^2 + N_\sigma^2} (-2\epsilon_* + 2\eta_*^{(\sigma)}), \end{aligned} \quad (\text{B9})$$

where $\eta^{(\sigma)} \equiv M_{\text{Pl}}^2 V_{\sigma\sigma} / V$ has been defined. Since the curvaton potential is rather flat, $\eta^{(\sigma)}$ should be highly suppressed. Moreover, ϵ_* should also be negligible in hilltop inflation models. Hence the expression for n_s can be simplified into

$$n_s \approx 1 + 2\eta_* \frac{1}{1 + 8r_{\text{dec}}^2 \epsilon_* M_{\text{Pl}}^2 / (3\sigma_{\text{inf}})^2}. \quad (\text{B10})$$

Non-Gaussianity. If the primordial fluctuations obey a strict Gaussian distribution, all statistical information is fully characterized by the two-point function. To be more concrete, all odd-point correlation functions vanish, while even-point functions can always be reduced to products of two-point functions. In this sense, the presence of a non-vanishing three-point function serves as a clear indicator of non-Gaussianity. In the δN formalism, a non-vanishing quadratic term may generate a nonzero three-point function. Schematically, one finds $\langle \zeta^3 \rangle \sim \langle \delta\varphi^i \delta\varphi^j \rangle \langle \delta\varphi^k \delta\varphi^l \rangle$, which implies that non-linear dependence of ζ on the field fluctuations could lead to non-Gaussianity [57–60].

The non-Gaussianity can be described by a dimensionless parameter f_{NL} , defined as

$$\begin{aligned} f_{\text{NL}} &\equiv \frac{5 N_i N_j N_{ij}}{6 (N_k N_k)^2} \\ &= \frac{5 N_\phi^2 N_{\phi\phi} + 2 N_\phi N_\sigma N_{\phi\sigma} + N_\sigma^2 N_{\sigma\sigma}}{6 (N_\phi^2 + N_\sigma^2)^2}. \end{aligned} \quad (\text{B11})$$

In the case where $N_{\phi\phi}$ is small and $N_{\phi\sigma}$ is negligible, f_{NL} is reduced to

$$f_{\text{NL}} \approx \frac{5 N_\sigma^2 N_{\sigma\sigma}}{6 (N_\phi^2 + N_\sigma^2)^2}. \quad (\text{B12})$$

To proceed, we need the explicit form of $N_{\sigma\sigma}$. Keeping in mind that r_{dec} also depends on σ_{inf} through $\rho_\sigma \propto \sigma_{\text{inf}}^2$, we have

$$N_{\sigma\sigma} = \frac{\partial}{\partial\sigma_{\text{inf}}} \left(\frac{2r_{\text{dec}}}{3\sigma_{\text{inf}}} \right) = \frac{2}{3} \left(\frac{r'_{\text{dec}}}{\sigma_{\text{inf}}} - \frac{r_{\text{dec}}}{\sigma_{\text{inf}}^2} \right), \quad (\text{B13})$$

with $r'_{\text{dec}} \equiv \partial r_{\text{dec}}/\partial\sigma_{\text{inf}}$. Using the definition of r_{dec} given in eq. (B4), one finds

$$N_{\sigma\sigma} = \frac{2r_{\text{dec}}}{9\sigma_{\text{inf}}^2} \left(3 - 4r_{\text{dec}} - 2r_{\text{dec}}^2 \right). \quad (\text{B14})$$

Therefore, we eventually arrive at

$$f_{\text{NL}} \approx \left(\frac{N_\sigma^2}{N_\phi^2 + N_\sigma^2} \right)^2 \left(\frac{5}{4r_{\text{dec}}} - \frac{5}{3} - \frac{5}{6}r_{\text{dec}} \right), \quad (\text{B15})$$

where we should note that $A_s^{\text{curv}} = H_*^2 N_\sigma^2 / (2\pi)^2$ and $A_s^{\text{inf}} = H_*^2 N_\phi^2 / (2\pi)^2$.

Appendix C: Viability of the cubic hilltop case

In this appendix, we explain why the sub-Planckian *cubic* hilltop case cannot be rescued by the curvaton mechanism in our benchmark setup. As we have mentioned in the main text, the main difficulty arises from the curvaton condition $|V_{\sigma\sigma}| \lesssim H^2$. For the *cubic* hilltop model, using $\phi_e^2 \simeq \mu^6 / (36M_{\text{Pl}}^4)$ and $\sigma_{\text{inf}} \simeq \sigma_t$ with

$$\sigma_t = \sigma_c \left(1 + \frac{B_3}{m_\phi^2} \right)^{1/4}, \quad \sigma_c^2 = \frac{m_\phi M_{\text{Pl}}}{\lambda}, \quad (\text{C1})$$

from $|V_{\sigma\sigma}| \lesssim H^2$ one finds

$$\frac{\lambda m_\phi \mu^6}{6M_{\text{Pl}}^5} \left(1 + \frac{B_3}{m_\phi^2} \right)^{1/2} \lesssim \frac{\Lambda^4}{3M_{\text{Pl}}^2}, \quad (\text{C2})$$

where m_σ^2 has been omitted from $|V_{\sigma\sigma}|$. Hence λ should obey the following upper bound

$$\lambda \lesssim \frac{2\Lambda^4 M_{\text{Pl}}^3}{m_\phi \mu^6 (1 + B_3/m_\phi^2)^{1/2}}. \quad (\text{C3})$$

From Eq. (44a), we have

$$A_s^{\text{inf}} \approx \frac{3N_e^4 M_{\text{Pl}}^2 \Lambda^4}{4\pi^2 \mu^6}. \quad (\text{C4})$$

With the help of the above equation, the upper bound on λ can be rewritten as

$$\lambda \lesssim \frac{8\pi^2 M_{\text{Pl}}}{3N_e^4 m_\phi (1 + B_3/m_\phi^2)^{1/2}} A_s^{\text{inf}}. \quad (\text{C5})$$

For our benchmark values $m_\phi = 3 \times 10^{-11} M_{\text{Pl}}$ and $m_\sigma = 5 \times 10^{-12} M_{\text{Pl}}$, and requiring $A_s^{\text{inf}} \sim 10^{-9}$, this gives

$$\lambda \lesssim \frac{10^{-4}}{(1 + B_3/m_\phi^2)^{1/2}} \lesssim 10^{-4}. \quad (\text{C6})$$

One should note that although the upper bound in eq. (C5) appears to scale as $\lambda \propto m_\phi^{-1}$, this does not imply that one can evade the constraint by taking m_ϕ arbitrarily small. Indeed, once $m_\phi^2 \ll B_3$, one has $(1 + B_3/m_\phi^2)^{1/2} \simeq (B_3)^{1/2}/m_\phi$. This inverse dependence on m_ϕ cancels the explicit factor of m_ϕ in σ_c^2 , so that σ_t becomes approximately independent of m_ϕ . The bound on λ then saturates to a value independent of m_ϕ , showing that lowering m_ϕ does not help to restore a sizable curvaton contribution.

On the other hand, the ratio between the curvaton and inflaton contributions to the scalar spectrum is

$$\frac{A_s^{\text{curv}}}{A_s^{\text{inf}}} \approx \frac{4\lambda\mu^6}{81N_e^4 m_\phi M_{\text{Pl}}^5}. \quad (\text{C7})$$

Since $\mu < M_{\text{Pl}}$ and λ is bounded as above, one obtains the conservative upper bound $A_s^{\text{curv}}/A_s^{\text{inf}} \lesssim 10^{-2}$. Therefore, in the sub-Planckian *cubic* hilltop case, the curvaton contribution can at most be at the few-percent level and is, in general, much smaller. The inflaton contribution thus dominates the total scalar spectrum, and the prediction for n_s remains essentially that of the single-field *cubic* hilltop model.

We have also performed a full numerical scan of the *cubic* case. The results show that the posterior distribution of n_s is sharply concentrated around $n_s \simeq 0.93$, which is precisely the characteristic prediction of the single-field sub-Planckian *cubic* hilltop model for $N_* = 55$. This confirms the validity of the above analytical estimate, and further demonstrates that the inclusion of the curvaton is insufficient to bring the sub-Planckian *cubic* hilltop model into agreement with observations.

For the trans-Planckian case of *cubic* hilltop inflation, the results are similar to those of *quartic* trans-Planckian hilltop inflation. In this regime, the end of inflation is no longer determined by the condition $|\eta| = 1$, but instead by $\epsilon = 1$. The inflationary observables n_s and r are then governed by eqs. (53a) and (53b) with $p = 3$. In the limit $\mu \gg M_{\text{Pl}}$, the single-field *cubic* hilltop model in the trans-Planckian case can already be compatible with current observations, and it typically predicts a sizable tensor-to-scalar ratio r . Once the curvaton is included, for the trans-Planckian case of *cubic* hilltop inflation, the value of r can be suppressed, so that both n_s and r can simultaneously lie within the 68% credible regions preferred by the P-ACT-LB-BK18 and Planck-LB-BK18 data. In summary, the resulting $n_s - r$ predictions for the trans-Planckian case of *cubic* hilltop inflation are qualitatively similar to those shown in Fig. 4 for the *quartic* hilltop trans-Planckian case. Thus, we do not display the results for the trans-Planckian case of *cubic* hilltop inflation sep-

arately since the plot would be very similar to Fig. 4 for the *quartic* hilltop trans-Planckian case.

-
- [1] P. A. R. Ade *et al.* (Planck), “Planck 2013 results. XXII. Constraints on inflation,” *Astron. Astrophys.* **571**, A22 (2014), arXiv:1303.5082 [astro-ph.CO].
- [2] Y. Akrami *et al.* (Planck), “Planck 2018 results. X. Constraints on inflation,” *Astron. Astrophys.* **641**, A10 (2020), arXiv:1807.06211 [astro-ph.CO].
- [3] Y. Akrami *et al.* (Planck), “Planck 2018 results. IX. Constraints on primordial non-Gaussianity,” *Astron. Astrophys.* **641**, A9 (2020), arXiv:1905.05697 [astro-ph.CO].
- [4] Alexei A. Starobinsky, “A New Type of Isotropic Cosmological Models Without Singularity,” *Phys. Lett. B* **91**, 99–102 (1980).
- [5] Alan H. Guth, “The Inflationary Universe: A Possible Solution to the Horizon and Flatness Problems,” *Phys. Rev. D* **23**, 347–356 (1981).
- [6] Andrei D. Linde, “A New Inflationary Universe Scenario: A Possible Solution of the Horizon, Flatness, Homogeneity, Isotropy and Primordial Monopole Problems,” *Phys. Lett. B* **108**, 389–393 (1982).
- [7] Andreas Albrecht and Paul J. Steinhardt, “Cosmology for Grand Unified Theories with Radiatively Induced Symmetry Breaking,” *Phys. Rev. Lett.* **48**, 1220–1223 (1982).
- [8] Thibaut Louis *et al.* (ACT), “The Atacama Cosmology Telescope: DR6 Power Spectra, Likelihoods and Λ CDM Parameters,” (2025), arXiv:2503.14452 [astro-ph.CO].
- [9] Renata Kallosh, Andrei Linde, and Diederik Roest, “ACT, SPT, and chaotic inflation,” (2025), arXiv:2503.21030 [hep-th].
- [10] Shuntaro Aoki, Hajime Otsuka, and Ryota Yanagita, “Higgs-modular inflation,” *Phys. Rev. D* **112**, 043505 (2025), arXiv:2504.01622 [hep-ph].
- [11] Arjun Berera, Suddhasattwa Brahma, Zizang Qiu, Rudnei O. Ramos, and Gabriel S. Rodrigues, “The early universe is ACT-ing warm,” (2025), arXiv:2504.02655 [hep-th].
- [12] Christian DiGuardi, Antonio J. Iovino, and Antonio Racioppi, “Fractional attractors in light of the latest ACT observations,” *Phys. Lett. B* **868**, 139664 (2025), arXiv:2504.02809 [gr-qc].
- [13] Ioannis D. Gialamas, Alexandros Karam, Antonio Racioppi, and Martti Raidal, “Has ACT measured radiative corrections to the tree-level Higgs-like inflation?” (2025), arXiv:2504.06002 [astro-ph.CO].
- [14] Alberto Salvio, “Independent connection in action during inflation,” *Phys. Rev. D* **112**, L061301 (2025), arXiv:2504.10488 [hep-ph].
- [15] Christian DiGuardi and Alexandros Karam, “Palatini linear attractors are back in action,” *Phys. Rev. D* **111**, 123521 (2025), arXiv:2504.12937 [gr-qc].
- [16] Minxi He, Muzi Hong, and Kyohei Mukaida, “Increase of n_s in regularized pole inflation & Einstein-Cartan gravity,” *JCAP* **09**, 080 (2025), arXiv:2504.16069 [astro-ph.CO].
- [17] Manuel Drees and Yong Xu, “Refined predictions for Starobinsky inflation and post-inflationary constraints in light of ACT,” *Phys. Lett. B* **867**, 139612 (2025), arXiv:2504.20757 [astro-ph.CO].
- [18] Jinsu Kim, Xinpeng Wang, Ying-li Zhang, and Zhongzhou Ren, “Enhancement of primordial curvature perturbations in R^{-3} -corrected Starobinsky-Higgs inflation,” *JCAP* **09**, 011 (2025), arXiv:2504.12035 [astro-ph.CO].
- [19] Ioannis D. Gialamas, Theodoros Katsoulas, and Kyrriakos Tamvakis, “Keeping the relation between the Starobinsky model and no-scale supergravity ACTIVE,” *JCAP* **09**, 060 (2025), arXiv:2505.03608 [gr-qc].
- [20] Ignatios Antoniadis, John Ellis, Wenqi Ke, Dimitri V. Nanopoulos, and Keith A. Olive, “How accidental was inflation?” *JCAP* **08**, 090 (2025), arXiv:2504.12283 [hep-ph].
- [21] Lang Liu, Zhu Yi, and Yungui Gong, “Reconciling Higgs Inflation with ACT Observations through Reheating,” (2025), arXiv:2505.02407 [astro-ph.CO].
- [22] D. S. Zharov, O. O. Sobol, and S. I. Vilchinskii, “Reheating ACTs on Starobinsky and Higgs inflation,” (2025), arXiv:2505.01129 [astro-ph.CO].
- [23] Yogesh, Abolhassan Mohammadi, Qiang Wu, and Tao Zhu, “Starobinsky like inflation and EGB Gravity in the light of ACT,” *JCAP* **10**, 010 (2025), arXiv:2505.05363 [astro-ph.CO].
- [24] Andrea Addazi, Yermek Aldabergenov, and Sergei V. Ketov, “Curvature corrections to Starobinsky inflation can explain the ACT results,” *Phys. Lett. B* **869**, 139883 (2025), arXiv:2505.10305 [gr-qc].
- [25] Wen Yin, “Higgs-like inflation ACTIVated mass,” *JCAP* **09**, 062 (2025), arXiv:2505.03004 [hep-ph].
- [26] Christian T. Byrnes, Marina Cortés, and Andrew R. Liddle, “The curvaton ACTs again,” (2025), arXiv:2505.09682 [astro-ph.CO].
- [27] Jeonghak Han, Hyun Min Lee, and Jun-Ho Song, “Higgs pole inflation with loop corrections in light of ACT results,” (2025), arXiv:2506.21189 [hep-ph].
- [28] Abolhassan Mohammadi, Yogesh, and Anzhong Wang, “Power Law Plateau Inflation and Primary Gravitational Waves in the light of ACT,” (2025), arXiv:2507.06544 [astro-ph.CO].
- [29] Monika Lynker and Rolf Schimrigk, “ACT Implications for Hilltop Inflation,” (2025), arXiv:2507.15076 [astro-ph.CO].
- [30] Venus Keus and Stephen F. King, “Chaotic Inflation RIDES Again,” (2025), arXiv:2511.05799 [hep-ph].
- [31] K. I. Izawa and T. Yanagida, “Natural new inflation in broken supergravity,” *Phys. Lett. B* **393**, 331–336 (1997), arXiv:hep-ph/9608359.
- [32] Vedat Nefer Senoguz and Q. Shafi, “New inflation, pre-inflation, and leptogenesis,” *Phys. Lett. B* **596**, 8–15 (2004), arXiv:hep-ph/0403294.
- [33] Lotfi Boubekeur and David H. Lyth, “Hilltop inflation,” *JCAP* **07**, 010 (2005), arXiv:hep-ph/0502047.
- [34] Stephen F. King and Xin Wang, “Modular invariant hilltop inflation,” *JCAP* **07**, 073 (2024), arXiv:2405.08924 [hep-ph].
- [35] Gui-Jun Ding, Si-Yi Jiang, and Wenbin Zhao, “Modular invariant slow roll inflation,” *JCAP* **10**, 016 (2024), arXiv:2405.06497 [hep-ph].

- [36] Stefan Antusch, David Nolde, and Stefano Orani, “Hill-top inflation with preinflation from coupling to matter fields,” *JCAP* **05**, 034 (2014), arXiv:1402.5328 [hep-ph].
- [37] Andrei D. Linde and Viatcheslav F. Mukhanov, “Non-gaussian isocurvature perturbations from inflation,” *Phys. Rev. D* **56**, R535–R539 (1997), arXiv:astro-ph/9610219.
- [38] David H. Lyth and David Wands, “Generating the curvature perturbation without an inflaton,” *Phys. Lett. B* **524**, 5–14 (2002), arXiv:hep-ph/0110002.
- [39] Takeo Moroi and Tomo Takahashi, “Effects of cosmological moduli fields on cosmic microwave background,” *Phys. Lett. B* **522**, 215–221 (2001), [Erratum: *Phys.Lett.B* 539, 303–303 (2002)], arXiv:hep-ph/0110096.
- [40] Takeo Moroi and Tomo Takahashi, “Cosmic density perturbations from late decaying scalar condensations,” *Phys. Rev. D* **66**, 063501 (2002), arXiv:hep-ph/0206026.
- [41] David H. Lyth, Carlo Ungarelli, and David Wands, “The Primordial density perturbation in the curvaton scenario,” *Phys. Rev. D* **67**, 023503 (2003), arXiv:astro-ph/0208055.
- [42] Alexei A. Starobinsky and Junichi Yokoyama, “Equilibrium state of a selfinteracting scalar field in the De Sitter background,” *Phys. Rev. D* **50**, 6357–6368 (1994), arXiv:astro-ph/9407016.
- [43] Kari Enqvist, Rose N. Lerner, Olli Taanila, and Anders Tranberg, “Spectator field dynamics in de Sitter and curvaton initial conditions,” *JCAP* **10**, 052 (2012), arXiv:1205.5446 [astro-ph.CO].
- [44] Robert J. Hardwick, Vincent Vennin, Christian T. Byrnes, Jesús Torrado, and David Wands, “The stochastic spectator,” *JCAP* **10**, 018 (2017), arXiv:1701.06473 [astro-ph.CO].
- [45] Andrei D. Linde, “Eternally Existing Selfreproducing Chaotic Inflationary Universe,” *Phys. Lett. B* **175**, 395–400 (1986).
- [46] Tom Rudelius, “Conditions for (No) Eternal Inflation,” *JCAP* **08**, 009 (2019), arXiv:1905.05198 [hep-th].
- [47] John R. Ellis, Andrei D. Linde, and Marc Sher, “Vacuum stability, wormholes, cosmic rays and the cosmological bounds on $m(t)$ and $m(H)$,” *Phys. Lett. B* **252**, 203–211 (1990).
- [48] Andrei D. Linde, “Hard art of the universe creation (stochastic approach to tunneling and baby universe formation),” *Nucl. Phys. B* **372**, 421–442 (1992), arXiv:hep-th/9110037.
- [49] J. R. Espinosa, G. F. Giudice, and A. Riotto, “Cosmological implications of the Higgs mass measurement,” *JCAP* **05**, 002 (2008), arXiv:0710.2484 [hep-ph].
- [50] Naoya Kitajima, Yuichiro Tada, and Fuminobu Takahashi, “Stochastic inflation with an extremely large number of e -folds,” *Phys. Lett. B* **800**, 135097 (2020), arXiv:1908.08694 [hep-ph].
- [51] Chiara Animali and Vincent Vennin, “Primordial black holes from stochastic tunnelling,” *JCAP* **02**, 043 (2023), arXiv:2210.03812 [astro-ph.CO].
- [52] P. A. R. Ade *et al.* (BICEP, Keck), “Improved Constraints on Primordial Gravitational Waves using Planck, WMAP, and BICEP/Keck Observations through the 2018 Observing Season,” *Phys. Rev. Lett.* **127**, 151301 (2021), arXiv:2110.00483 [astro-ph.CO].
- [53] David Langlois and Filippo Vernizzi, “Mixed inflaton and curvaton perturbations,” *Phys. Rev. D* **70**, 063522 (2004), arXiv:astro-ph/0403258.
- [54] George Lazarides, Roberto Ruiz de Austri, and Roberto Trotta, “Constraints on a mixed inflaton and curvaton scenario for the generation of the curvature perturbation,” *Phys. Rev. D* **70**, 123527 (2004), arXiv:hep-ph/0409335.
- [55] Kazuhide Ichikawa, Teruaki Suyama, Tomo Takahashi, and Masahide Yamaguchi, “Primordial Curvature Fluctuation and Its Non-Gaussianity in Models with Modulated Reheating,” *Phys. Rev. D* **78**, 063545 (2008), arXiv:0807.3988 [astro-ph].
- [56] Misao Sasaki and Ewan D. Stewart, “A General analytic formula for the spectral index of the density perturbations produced during inflation,” *Prog. Theor. Phys.* **95**, 71–78 (1996), arXiv:astro-ph/9507001.
- [57] David H. Lyth and Yeinzon Rodriguez, “The Inflationary prediction for primordial non-Gaussianity,” *Phys. Rev. Lett.* **95**, 121302 (2005), arXiv:astro-ph/0504045.
- [58] Eiichiro Komatsu and David N. Spergel, “Acoustic signatures in the primary microwave background bispectrum,” *Phys. Rev. D* **63**, 063002 (2001), arXiv:astro-ph/0005036.
- [59] N. Bartolo, E. Komatsu, Sabino Matarrese, and A. Riotto, “Non-Gaussianity from inflation: Theory and observations,” *Phys. Rept.* **402**, 103–266 (2004), arXiv:astro-ph/0406398.
- [60] Xingang Chen, “Primordial Non-Gaussianities from Inflation Models,” *Adv. Astron.* **2010**, 638979 (2010), arXiv:1002.1416 [astro-ph.CO].
- [61] P. A. R. Ade *et al.* (Planck), “Planck 2015 results. XX. Constraints on inflation,” *Astron. Astrophys.* **594**, A20 (2016), arXiv:1502.02114 [astro-ph.CO].
- [62] E. Allys *et al.* (LiteBIRD), “Probing Cosmic Inflation with the LiteBIRD Cosmic Microwave Background Polarization Survey,” *PTEP* **2023**, 042F01 (2023), arXiv:2202.02773 [astro-ph.IM].
- [63] Clarence L. Chang *et al.*, “Snowmass2021 Cosmic Frontier: Cosmic Microwave Background Measurements White Paper,” (2022), arXiv:2203.07638 [astro-ph.CO].
- [64] Erminia Calabrese *et al.* (Atacama Cosmology Telescope), “The Atacama Cosmology Telescope: DR6 constraints on extended cosmological models,” *JCAP* **11**, 063 (2025), arXiv:2503.14454 [astro-ph.CO].
- [65] Alexei A. Starobinsky, “STOCHASTIC DE SITTER (INFLATIONARY) STAGE IN THE EARLY UNIVERSE,” *Lect. Notes Phys.* **246**, 107–126 (1986).
- [66] David H. Lyth, Karim A. Malik, and Misao Sasaki, “A General proof of the conservation of the curvature perturbation,” *JCAP* **05**, 004 (2005), arXiv:astro-ph/0411220.